**Sofia University "St. Kliment Ohridski"**
**Faculty of Chemistry and Pharmacy**
**Department of Chemical and Pharmaceutical Engineering**

*Diana Peychova Cholakova*

# *Spontaneous deformations of emulsion drops undergoing phase transitions*

## SUMMARY

**of the THESIS submitted**

**for the degree**

**"Doctor of Philosophy" (PhD)**

**Specialty:**

**4.2 Chemical sciences (Physical chemistry – Macrokinetics)**

**Supervisor:**

**Prof. Nikolai D. Denkov**

**Sofia, 2020**

This Thesis contains 128 pages, 54 figures, 9 tables, 21 equations and 142 references.

Numbering of the sections, figures, tables, equations and references in the current Summary follows the numbering in the Thesis. The list of references is available in the Thesis.

# Contents of the Summary

# Chapter I. Introduction

## 1.1 Basic concepts

### 1.1.1 *Emulsions*

Emulsions are disperse systems of two immiscible liquids in which one of the liquids (*disperse phase*) is dispersed as droplets in the other liquid (*disperse medium*). Upon mixing of the two liquids (*emulsification*), the contact area between the two phases increases multiple times which defines the emulsions as *thermodynamically unstable* systems:

$$\Delta U = \gamma \Delta S = \gamma \left( S_f - S_i \right) \tag{1}$$

where γ is the interfacial tension of the water-oil interface, $\Delta U$ denotes the increase in the internal energy of the system, $\Delta S = S_f - S_i$ is the change of the interfacial area between the oil and water phases, $S_i$ – initial contact area before mixing, $S_f$ – contact area after mixing, and.

### 1.1.2 *Surfactants;*

To stabilize for long periods the thermodynamically unstable emulsions (*kinetic stabilization*), surface active substances (surfactants) are usually added. Surfactant molecules have amphiphilic nature – they contain both hydrophilic and hydrophobic fragments. Therefore, surfactant molecules adsorb spontaneously on the oil-water interface, decreasing the interfacial tension and stabilizing the emulsion drops against coalescence.

### 1.1.3 *Capillary pressure*

The pressure jump across the interface between two fluid phases is called *capillary pressure*, $p_c$.[2,4] Capillary pressure is caused by the molecular forces acting at the interface.[2,4] For an oily drop immersed in aqueous surfactant solution, the capillary pressure is defined as the difference in the pressures inside and outside the drop:

$$p_c = \frac{4\gamma}{d}, \tag{2}$$

where γ is interfacial tension and $d$ is drop diameter.[2,4] Because $p_c$ is inversely proportional to the drop size, smaller droplets have higher capillary pressure and vice versa.

### 1.2 Spontaneous deformations of emulsion droplets upon cooling

One of the main principles determining the processes in nature is the principle of energy minimization. In the absence of external forces, the systems acquire the states with minimal energy (minimum of the respective characteristic thermodynamic function). This principle is reflected in the spherical shape of the small emulsion droplets – this is the shape with smallest interfacial energy. Respectively, upon freezing, such drops crystallize usually into frozen particles with spherical or close to spherical shape.[8]

The process of spontaneous deformation of emulsion droplets upon cooling was observed initially in our previous study, published in 2015 in *Nature*.[10] There we showed that emulsion droplets of various linear alkanes with chain lengths varied between 14 and 20 carbon (C) atoms, dispersed in aqueous surfactant solutions, change their shape upon cooling and form various non-spherical regular shapes, such as hexagonal, triangular and tetragonal platelets and rod-like particles, Figure 2 in the Thesis (see also Figures 21 and 23 below).

In our previous experiments we showed that the final drop shape upon freezing depends on the specific surfactant, the initial drop size and the rate of cooling. The role of these factors was studied qualitatively only, while quantitative data was not obtained. These factors were studied in more detail in a subsequent study which is presented as Chapter III in the current Thesis.

Based on the results from our initial experiments, we proposed the following mechanism of the process of spontaneous drop-shape deformations observed upon cooling.[10] The experiment showed that, to observe any drop shape change prior to drop freezing, surfactant molecules with tails similar or longer than the alkane chain were required. This requirement shows that, most probably, the observed shape transformations are trigged by the freezing of the surfactant adsorption layers, formed on the surface of the fluid drops. However, the numerical estimates showed that the frozen adsorption monolayers do not possess a sufficiently high bending moment to deform the hydrocarbon drops. Therefore a multilayer of intermediate rotator phase (plastic phase) should be formed next to the surface of the liquid drops to cause the observed drop shape transformations before their final freezing. *Rotator phases* are known to exist for long-chain bulk alkanes at intermediate temperatures, between their fully disordered liquid state and the completely ordered crystalline state.[11-14]

The simplest possible explanation of the observed drop deformations would be that the frozen adsorption layer induces structuring inside the entire drop volume. However, the optical observations do not support this simplest explanation. Therefore, we concluded that the freezing surfactant adsorption layer induces the formation of a thin layer of a hydrocarbon plastic rotator

phase next to the drop surface, and this thin layer of rotator phase drives the observed drop-shape changes. Figure 4 in the Thesis shows schematically the proposed mechanism. The presence of long range positional order in the rotator phase generates sufficiently high anisotropic stresses, able to counteract the capillary pressure of the drop surface and, thus, to cause drop shape changes. The thickness of the ordered layer is smaller than 1 μm and, therefore, in polarized light the deformed drops have only faint colors at their edges. If the interior of the droplets were entirely filled with anisotropic plastic phase, the liquid drop would appear as having bright colors in cross-polarized light, as observed with frozen alkane particles or with the fully plastisized mixed alkane particles, filled with structured rotator phase.[17] The plastic rotator phase, formed on the drop surface, allows formation of non-spherical drops which would not be stable otherwise, for example triangular platelets with long asperities and tetragonal particles with hole in their center, see Figure 3 for example.

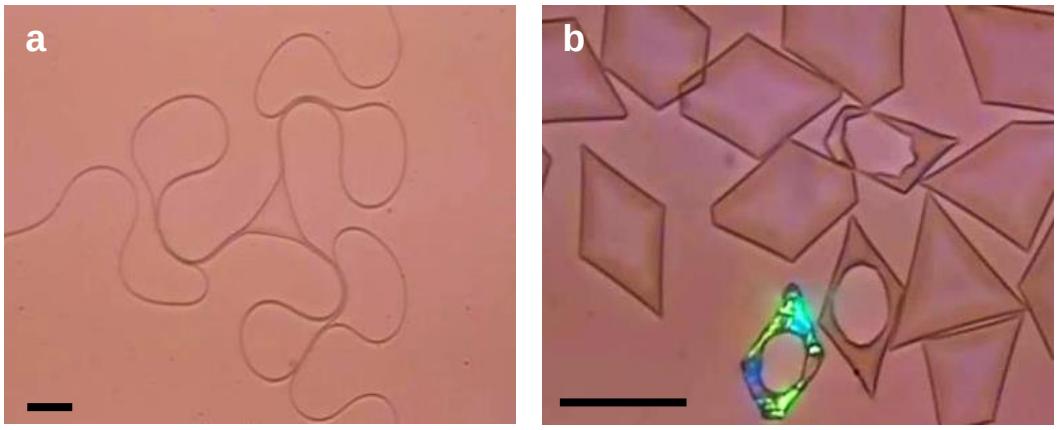


**Figure 3**. Examples of fluid non-spherical drops which would not be stable in shape in the absence of elasto-plastic material on the drop surface: (a) Triangular platelet with long cylindrical asperities. (b) Rhomboid-shaped fluid platelets. Two platelets with holes in their center are seen - a shape which would be unstable for fully liquid drops. The colored particle at the bottom of the image is the only one frozen here. Scale bars: 50 μm. Figure is adapted from Ref. [10].

The experiments conducted for the current Thesis are meant to upgrade significantly our previous work, summarized briefly above.[10] The current study aims to deepen our understanding of the role of different factors in the process of spontaneous drop shape transformations, observed upon cooling.[10] For this purpose, we studied various oil-surfactant systems not only qualitatively, but also characterized them quantitatively. We studied also in detail the initially proposed mechanism by using several quantitative and structural methods, aiming to verify unambiguously the formation of plastic rotator phases on the drop surface, prior to drop crystallization. The results from these measurements are used also to determine the thickness of the layer of rotator phase on the surface of various non-spherical drops.

## 1.3 Rotator phases in alkane systems

### *1.3.1 Crystal structures of solid bulk alkanes*

Bulk alkanes crystallize into several different *crystalline lattices* depending on the length of the alkane molecules. The even-numbered alkanes with chain length between 14 and 24 C-atoms form triclinic crystal lattice, between 26 and 38 C-atoms – monoclinic lattice, and between 40 and 66 C-atoms – orthorhombic crystal lattice.[24] In contrast, the odd-numbered alkanes with chain length between 13 and 41 C-atoms form orthorhombic lattice, while the shorter-chain odd-numbered alkanes crystallize in triclinic lattice.[24]

### *1.3.2 Types of rotator phases*

*Rotator phases* are intermediate phases between the completely ordered crystalline phase and the fully disordered, isotropic liquid phase.[11-13] Molecules in the rotator phase have long-range positional order in the three dimensional space, while they have a significant freedom with respect to their molecular rotation (therefore, they are called "rotator phases").[11-14] These phases are also called "plastic phases" because they exhibit complex visco-plastic rheological behavior, due to the intrinsic significant mobility of the alkane molecules.[13,22,26,27] These phases are also called "highly ordered smectics".[13,26,27]

The term "rotator phase" is mainly used for alkanes, but phases with similar properties have been observed also with various other substances, composed of molecules which contain linear alkyl chains. Examples are 1-alkenes[39], *n*-alcohols[40], asymmetric alkanes (alkyl cyclohexanes)[41] and others[42-46]. Furthermore, as clarified by Small[23], the most thermodynamically unstable polymorphic modification formed upon crystallization of triglycerides, the so-called "α-phase", has properties which are very similar to those of the rotator phases. Similar intermediate phases are known to form also with long chain fatty acids and phospholipids.[23]

**Table 3.** Main structural characteristics of the rotator phases in alkanes. Data from Ref. [13].

| Rotator phase | D | $\Phi_d$ | $\theta$ | $\Phi_t$ | Layer structure | Lattice | Carbon number |
|---|---|---|---|---|---|---|---|
| $R_I$ | Large | 0 | 0 | - | ABABAB… | Face centered orthorhombic | $n \leq 25$ |
| $R_{II}$ | 0 | - | 0 | - | ABCABC… | Rhombohedral | $22 \leq n \leq 26$ |
| $R_{III}$ | Small | > 0 | > 0 | > 0 | AAA… | Triclinic | $n \geq 27$ |
| $R_{IV}$ | Small | 0 | > 0 | 0 | AAA… | Monoclinic | $26 \leq n \leq 30$ |
| $R_V$ | Large | 0 | > 0 | 0 | ABABAB… | Face centered orthorhombic | $23 \leq n \leq 27$ |

Upon cooling of bulk alkanes, **five different rotator phases** may be observed depending on the alkane chain-length. These phases are denoted as $\boldsymbol{R_x}$, where the subscript „***x***“ is a Roman number between one and five.[13,14,47] The rotator phases differ from one another by: the type of crystal lattice formed by the alkane molecules, the tilt angle with respect to the planes in the lamellar structure, and the direction of tilting with respect to the neighbors, see Table 3.

### *1.3.3 Thermodynamic stability of the rotator phases*

Depending on the alkane chain-length, one or several consecutive rotator phases may be observed upon cooling, see Figure 9.[13,14,22,30-33,38-52]

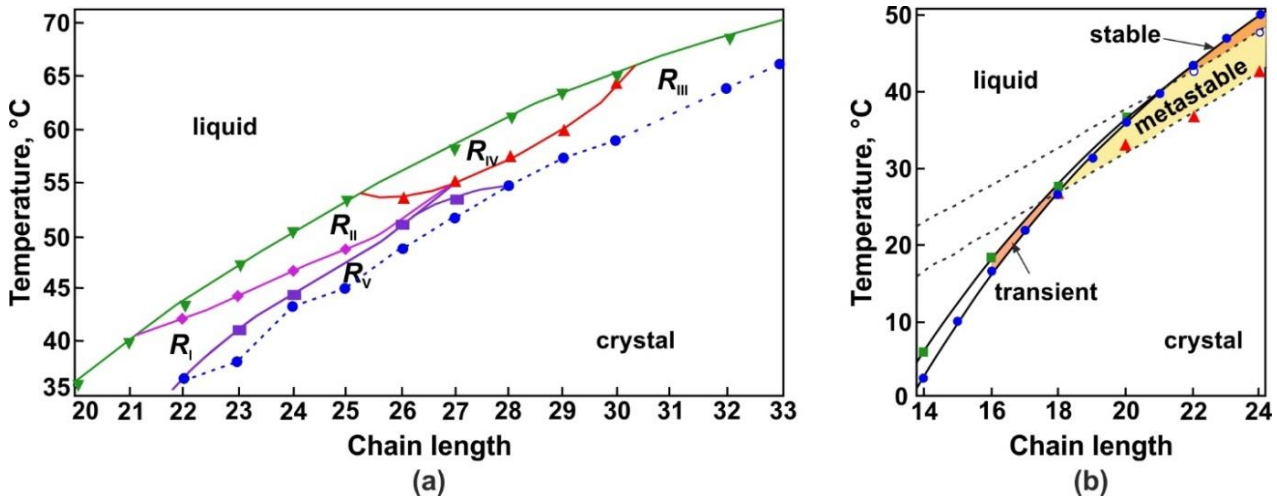


**Figure 9.** Phase diagrams for alkanes with different chain lengths, observed upon cooling.[13,30]

Depending on stability of the rotator phases, they are classified as thermodynamically stable, metastable or transient.[13,30] Thermodynamically stable rotator phases are observed upon both alkane cooling and alkane heating. Upon cooling, they are formed at a temperature which is higher than the temperature of the phase transition liquid → crystal, $T_{L\rightarrow T}$. Metastable rotator phases form upon cooling at a temperature lower than $T_{L\rightarrow T}$ and exist in a narrow temperature range, while the transient rotator phases form after significant undercooling and exist very shortly (for seconds), facilitating the transition from liquid to crystalline phase. Both metastable and transient rotator phases are observed upon cooling only. The rotator phases formed in bulk even-numbered alkanes with chain length shorter than 22 C-atoms are characterized as metastable or transient, whereas the rotator phase formed in odd-numbered alkanes are usually thermodynamically stable.[30]

### *1.3.4 Surface rotator phases*

For most substances, a molten layer with molecular thickness is observed at the crystal-air interface, at temperatures which are up to several degrees lower than the bulk melting temperature of the respective solid substance, $T_m$. The molten surface layer wets the solid bulk material and is in thermodynamic equilibrium with the bulk substrate. This phenomenon, known in the literature as "surface melting", occurs on the surface of most known substances – metals, semiconductors, ice, molecular crystals, etc.[53,54]

The surface freezing, observed in alkanes and long chain alcohols is the opposite phenomenon. In this case, an ordered surface layer is formed on top of the liquid substrate, at temperatures which are up to 3.1°C higher than the bulk melting temperature of the substance, see Table 4 in the Thesis.[57,58]

Formation of ordered surface layers may be detected using several structural methods, incl. SAXS or GID, as well as with surface tension measurements at different temperatures. Studies at the alkane-vapor interface showed that an ordered surface layer is formed with a thickness equal to the length of a single alkane molecule, i.e. this is a monolayer.[58-61] A grazing incidence diffraction (GID) experiments showed that the molecules in the surface layer arrange in a hexagonal close packing with area-per-molecule similar to that in $R_{II}$ rotator phase.[58-61] Long-range positional order of the molecules in such surface layers was observed at distances > 1 μm.[60]

In interfacial tension measurements, a change in the slope of the $\gamma(T)$ dependence is observed upon surface freezing. The reason is that the entropy of the molecules in the ordered surface layer is smaller than the entropy of the molecules in the bulk phase – therefore, the slope of the curve $\gamma(T)$ changes from negative to positive upon layer freezing.

Interfacial freezing was not detected at the alkane-water interface.[65-68] Various studies show that the interfacial freezing may be induced if a long chain surfactant is added into the water phase. For example, interfacial freezing is observed with aqueous solutions of various cationic alkyl bromides ($C_n$TAB) surfactants.[66-76] These studies showed also that the increase of the surfactant concentration leads to higher temperature at which the surface freezing is observed.[66] Furthermore, it was shown that an increase of the temperature of surface freezing is observed also when the surfactant tail length is increased, as the tail length affects the freezing temperature of the surfactant adsorption layer at the oil-water interface, Figure 13b from the Thesis.

### *1.3.5 Rotator phases in confinements*

Confining alkanes in microcapsules, nanopores or micrometer sized emulsion droplets significantly increases the stability of the observed rotator phases and changes the temperature range in which these phases occur.[77-92]

For example, upon cooling of bulk hexadecane ($C_{16}$), only a short living transient rotator phase has been observed, Figure 9b[30], whereas if the hexadecane is confined in the pores of a Vycor glass matrix of amorphous $SiO_2$, a thermodynamically stable $R_I$ rotator phase was detected upon both cooling and heating.[79] Rotator phase $R_I$ was observed also with $C_{14}$ alkane confined in Vycor glass pores, but only upon cooling, i.e. the phase had metastable character. No rotator phase was observed with dodecane ($C_{12}$) or with shorter even alkanes.[79]

Cooling of alkanes confined in polymeric microcapsules, synthesized from melamine-formaldehyde resin, also showed prefered formation of rotator phases in this geometry, as compared to the bulk alkane samples.[83,84,88,90]

Rotator phases were detected also upon cooling of hexadecane emulsion droplets, dispersed in the aqueous solution of the nonionic surfactant Tween 40 which contains saturated $C_{16}$ tail.[103] The results in this study[103] showed that the ordered phase is mainly formed next to the drop surface, with preferred molecule orientation perpendicular to the surface. In contrast, when the hexadecane droplets were dispersed in Tween 80 solution (surfactant with double bond in the middle of the $C_{18}$ hydrophobic tail), bulk drop crystallization was observed without preferred orientation of the frozen molecules.[103]

The rotator phase formation in emulsion droplets affects significantly the rate of drop crystallization, as well. For example, it was shown that for samples, stabilized by Tween 40 ($C_{16}SorbEO_{20}$) or Tween 60 ($C_{18}SorbEO_{20}$), the initial rate of drop crystallization into solid triclinic phase was much faster, as compared to the one observed in similar emulsions, but stabilized by Tween 20 ($C_{12}SorbEO_{20}$) or Tween 80 ($C_{18:1}SorbEO_{20}$). This difference was explained with the different nucleation mechanisms in the two types of emulsions.[8,105] When no rotator phase is formed, the drops crystallize via homogeneous nucleation and much greater supercooling is needed for nuclei to form. In contrast, when rotator phases are formed at the drop surface, they act as templates for crystal nucleation and growth inside the drops, therefore the rates of alkane crystallization are much higher in this second case.[8,103-105]

## Aims of the study and structure of the Thesis:

This Thesis presents a systematic study of the process of spontaneous drop-shape deformations observed upon emulsion cooling. We performed experiments to clarify and quantify the role of the various factors for the observed process. Also, we performed a series of model experiments which helped us to clarify the mechanism of this process.

Main aims of the performed study are:

(1) To describe the role in the phenomenon studied of the cooling rate, the initial drop size, and the type of surfactant used for emulsion stabilization.
(2) To study in more detail the mechanism of drop shape deformations upon cooling.
(3) To develop a quantitative model for interpretation of the obtained experimental results which allowed us to determine the thickness of the surface layer of rotator phase in the various emulsion types.

The current Thesis is structured as follows:

Chapter II presents the methods and materials used.

Chapter III presents experimental results which clarify and quantify the role of the factors which can be used for control of the studied phenomenon.

Chapter IV presents experimental results, obtained with the aim to clarify the mechanism of spontaneous drop shape deformations upon cooling.

Chapter V presents the theoretical model developed with the aim to determine the thickness of the rotator phase, formed on the surface of the deformed drops.

The main results from each part of the study are summarized at the end of each chapter, and the main scientific contributions are summarized at the end of the Thesis.

# Chapter II. Materials and experimental methods

This chapter describes the materials and experimental methods used in conduction of the experiments, presented in Chapters III and IV of the Thesis.

## 2.1 Materials

### *2.1.1 Oils*

As disperse phase in the studied emulsions, as well as in the model experiments, we used mainly hexadecane, alkane with linear saturated chain of 16 C-atoms, $C_{16}$. It had purity ≥ 99% and was produced by Sigma-Aldrich.

To demonstrate that the drop self-shaping process is general and can be observed with various hydrophobic substances, we used also alkanes with various chain lengths between 10 and 20 C-atoms, see Table 5 in the Thesis, as well as long chain *n*-alcohols, 1-alkenes, pentadecyl-cyclohexane and others, see Table 7 in the Thesis.

### *2.1.2 Surfactants*

All aqueous surfactant solutions were prepared with deionized water with electrical resistivity > 18 MΩ.cm, purified by Elix 3 Module (Millipore).

For emulsion stabilization we used various nonionic surfactants belonging to two main classes: polyoxyethylene alkyl ethers with formula $C_nEO_m$ and polyoxyethylene sorbitan monoalkylates $C_nSorbEO_m$, where subscript *n* denotes the number of carbon atoms in the hydrophobic tail and *m* denotes the number of ethoxy units ($-CH_2CH_2O-$) in the hydrophilic head. "Sorb" indicates the presence of sorbitan ring in the hydrophilic head. The number *n* was varied between 12 and 18, and *m* was varied between 2 and 50.

In some of our experiments we used also two cationic surfactants $C_{18}TAB$ and $C_{16}TAB$ (alkyl trimethyl ammonium bromides with purity > 99%) and three anionic surfactants from the sodium alkyl sulfate series, with different lengths of their hydrophobic tails – between 12 and 18 C-atoms. All surfactants were used as received from the producer.

The surfactant concentration was 1.5 wt. % for all nonionic surfactants, except for $C_{16}EO_{10}$ and $C_{18}EO_{10}$ for which the concentration was 0.75 wt. %. The concentration of the cationic surfactant $C_{18}TAB$ was 0.02 wt. % and for the rest of the ionic surfactants – 1 wt. %. All working concentrations were chosen to be well above the critical micellizatyion concentrations (CMC) to ensure enough surfactant for adsorption on the expanding drop surface drop deformation.

## 2.2 Experimental methods

### *2.2.1 Emulsion preparation*

The studied emulsions were prepared by membrane emulsification.[114-116] The oily phase was emulsified by passing it through a porous glass membrane under pressure into the continuous phase (aqueous surfactant solution). Membranes with mean pore diameter between 1 and 10 μm were used to produce monodisperse emulsions with mean drop diameter between 3 and 33 μm respectively.[116]

### *2.2.2 Optical observations upon cooling*

To study the emulsion behavior upon cooling, we performed optical observation using AxioImager.M2m or AxioPlan microscope, Zeiss, Germany. In most experiments we placed the emulsion samples in a rectangular capillary of length 50 mm, width 1 or 2 mm, and height 0.1 mm. This capillary was enclosed within a custom-made metal cooling chamber, with optical windows for microscopy observation. The thermostatic chamber was connected to a thermostat (Julabo CF30) which allowed us to control precisely the temperature, see Figure 17a,b in Thesis. The temperature in the sample during the experiments was measured using a calibrated thermocouple probe, with an accuracy of ± 0.2°C. The thermocouple was inserted in one of the orifices of the aluminum thermostating chamber and mounted at a position where a capillary with the emulsion sample would be normally placed for microscope observations. In this way, the temperature on the position of sample location is measured.

To check the actual behavior of the drops in emulsion samples during the DSC experiments, we performed optical observations also with samples placed in DSC pans. The observed sample behavior was identical to the one observed in glass capillary (except for the explicitly described differences for the systems from *Group D*).

The optical observations were performed in cross-polarized white light, with included $\lambda$-compensator plate, situated after the sample and before the analyzer, at 45° with respect to both the analyzer and the polarizer. Under these conditions, the liquid background and the fluid objects have typical magenta color, whereas the frozen birefringent areas (polycrystallites) appear brighter and may have intense colors, Figure 18.[117,118] Long-focus objectives ×20, ×50 and ×100 were used. We used transmitted light when taking images for determination of the drop-size distribution.

To quantify the drop deformations along the cooling process, we used the drop aspect ratio, *AR*, defined as the ratio between the longest length of the observed two-dimensional projection of the drop, $l_{max}$, and the initial drop diameter, $d_{ini}$, viz. $AR = l_{max}/d_{ini}$, Figure 18.

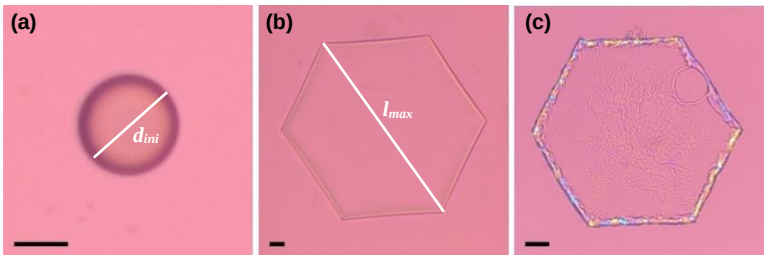


$$AR = \frac{l_{\max}}{d_{ini}}$$

**Figure 18. Illustrative microscopy images of an emulsion drop which deforms upon cooling.** In the beginning of the experiment, at high temperature, the drops are spherical (a). Upon cooling, the drops deform into various fluid non-spherical particles (b) and when the freezing temperature is reached, the drops freeze into solid particles (c). Under the described optical conditions, the fluid objects do not have colors (a,b), whereas the frozen objects (c) have bright colors. To quantify the drop deformations, we define the aspect ratio as the ratio between the longest 2D contour which can be measured in the deformed drop and the initial drop diameter, $AR = l_{\max} / d_{ini}$. Scale bars: 20 μm.

### *2.2.3 Determination of the initial drop size*

The initial drop diameter in the emulsions, $d_{ini}$, was determined using the ImageAnalysis Module of Axio Vision software (Zeiss, Germany). For each sample, the size of more than 10 000 individual droplets was measured and then the mean volume-surface drop diameter[4] was calculated, $d_{32} = \sum_i N_i d_i^3 / \sum_i N_i d_i^2$, where $N_i$ is the number of drops with diameter $d_i$. In the text we denote this diameter as initial drop size $d_{ini} = d_{32}$.

### *2.2.4 Interfacial tension measurements*

The hexadecane-water interfacial tension, γ, was measured by drop-shape analysis method on DSA 100 apparatus (Kruss, Germany). In this method, a millimeter sized oil drop is formed on the tip of a capillary which is immersed into the studied surfactant solution.[121-123] The drop shape profile is captured with video-camera. Then the interfacial tension is calculated from the drop profile using the Laplace equation of caillarity.[123] These experiments were performed with different temperature protocols and the data presented in the main text are from the experiments performed at constant cooling rate, varied between 0.1°C/min and 0.5°C/min, as these experiments represent best the conditions during the optical observations of self-shaping emulsion drops. TC40 thermostating cell was used to vary the temperature of the measured sample. In a separate complementary experiment we measured the exact temperature inside the cell using a calibrated

thermocouple probe and following the same temperature protocol as the one used during the interfacial tension measurements.

### *2.2.5 Differential scanning calorimetry (DSC) measurements*

The DSC experiments were performed on Discovery DSC 250 apparatus (TA Instruments, USA). In these experiments, the studied sample, with oil weight fraction varied between 0.3 and 10 wt. %, was weighted and placed into an aluminum hermetic DSC pan and then the pan was sealed with aluminum hermetic lid (TZero Pans & Hermetic lids). The samples were cooled and heated at 0.5°C/min rate, and the thermal data during both cooling and heating were recorded. To allow direct comparison between the various thermograms, in all figures in the Thesis, the thermograms were shifted in vertical direction so that the baseline value is set to zero, and the *y*-axis was rescaled so that the total peak area corresponds to the total bulk enthalpy of the melting oil, contained in the sample. The horizontal dashed line drawn in the thermograms are used as guides to the eye only.

### *2.2.6 Small angle X-ray scattering measurements (SAXS)*

To obtain a direct information about the molecular ordering inside the emulsion samples, we performed small angle X-ray scattering experiments. These experiments were performed in the synchrotron facilities Elettra, Triest, Italy (SAXS beamline) and Soleil, Paris, France (SWING beamline). The synchrotron radiation was needed because the observed processes are very dynamic and one needs to obtain sufficiently strong signal for a relatively short period of time (seconds to minutes).

During the measurements in Elettra synchrotron, we used X-ray beam with energy 8 keV and wavelength $\lambda \approx 1.55$ Å, whereas in Soleil the parameters were 16 keV, $\lambda \approx 0.78$ Å. For these measurements, the samples were placed inside cylindrical borosilicate capillaries with diameter 1 or 1.5 mm, length 80 mm and wall thickness of 10 μm. The capillaries were placed into a thermostating cooling chamber, similar to the one used in the microscopy observations. The experimental cell was mounted so that the beam passed through the studied emulsion sample. In Elettra, we performed all measurements at fixed cooling rate of 0.5°C/min, whereas in Soleil we cooled the sample to specific temperature using 0.5°C/min cooling rate and, afterwards, we hold this temperature for a given period of time and, finally, cooled or heated the sample depending on the purpose of the specific experiment.

# Chapter III. Control factors

## 3.1 Evolutionary scheme

In the current study, the initial drop shape evolutionary scheme, Figure 2a in the Thesis, was completed with some new drop shapes, observed in the additional experiments with different alkanes. The upgraded evolutionary scheme is presented in Figure 21.

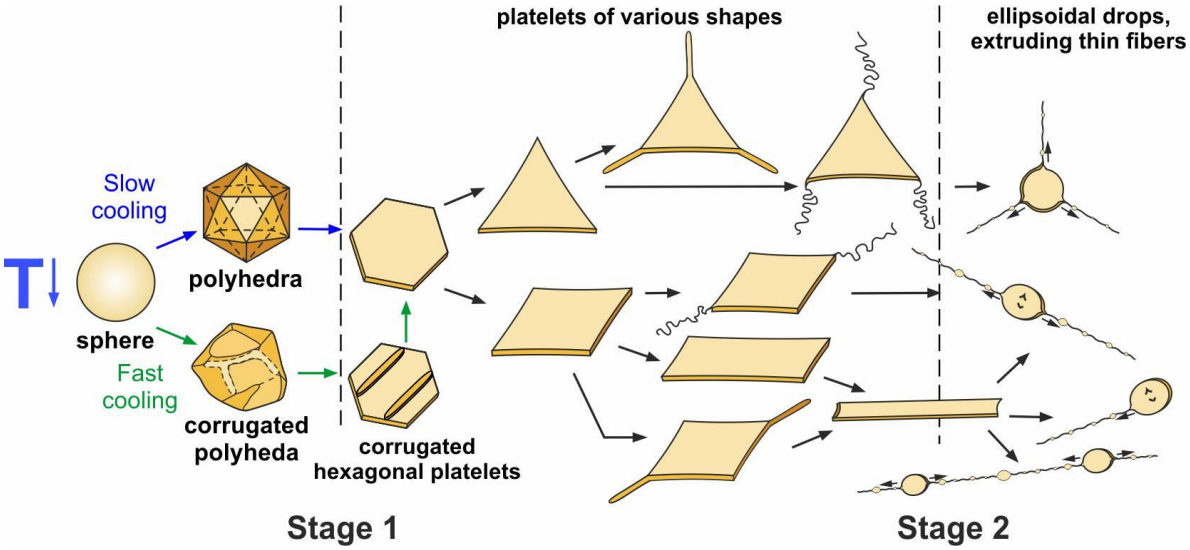


**Figure 21.** Evolutionary scheme, showing the main stages of the drop shape evolution observed upon cooling.

For a given system and cooling protocol, the observed deformations were well reproducible. Depending on the cooling rate and other factors discussed below, the deformed fluid droplets could freeze in any of the described evolutionary stages. Upon freezing, the fluid non-spherical droplets transform into frozen particles, preserving their non-spherical shape indefinitely in time, if stored at $T < T_m$. Illustrative images of drops with different shapes are shown in Figure 23.

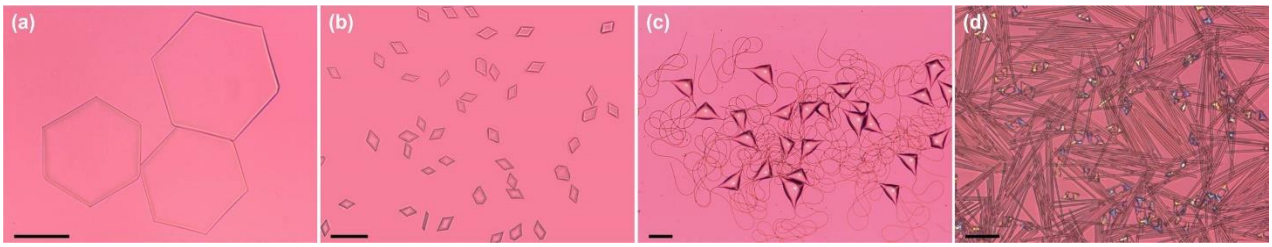


**Figure 23.** Fluid droplets with different non-spherical shapes: (a) hexagonal prisms, $C_{16}/C_{16}SorbEO_{20}$; (b) tetragonal prisms, $C_{16}/C_{18}SorbEO_{20}$; (c) particles with bacterial-like shapes, $C_{15}/C_{16}EO_{20}$ (d) rod-like fluid droplets and frozen tetragonal particles, $C_{18}/SorbEO_{20}$. Scale bars: 50 μm.

### 3.2 Spontaneous deformations of non-alkane droplets

Similar drop shape evolution was observed also with other hydrophobic substances, from classes known to form rotator plastic phases before complete crystallization. The substances tested included three long chain *n*-alcohols (number of C-atoms from 10 to 14), three tracylglycerides – trilaurin, trimyristin and tripalmitin, pentadecylcyclohexane, and two 1-alkenes with 17 and 20 C-atoms (heptadecene and eicosene). With all these substances we observed the same series of drop deformations as the one described above for alkane drops, Figure 24 in Thesis.

The role of the various factors, described below for alkanes, was the same in the experiments performed with non-alkane droplets. In all systems studied, the drop-shape evolution was more pronounced for smaller droplets, lower cooling rates, and larger difference between the lengths of the surfactant tail and the molecular chain of the oil.

### 3.3 Role of the difference between the chain-lengths of *n*-alkane and surfactant tail

In our experiments, we observed drop shape deformations before freezing only when the surfactant tail was longer, equal or by no more than 3 C-atoms shorter than the chain length of the dispersed alkane. For example, hexadecane ($C_{16}$) droplets stabilized by $C_{12}SorbEO_{20}$, $C_{12}EO_{23}$ or $C_{12}H_{25}SO_4Na$ did not change their shape upon cooling and the frozen drops had spherical or close to spherical shape. Drop shape deformation before freezing were not observed either if the surfactant had double bond in the middle of its hydrophobic tail. For example, $C_{16}$ drops dispersed in polyoxyethylene (20) sorbitan monooleate, $C_{18:1}SorbEO_{20}$ (Tween80) did not change their shape before freezing although the surfactant tail in this case was longer than the alkane chain. This is caused by the fact that the double bond in the surfactant tail disrupts the regular alignment and packing of the molecules in the adsorption layer. As a result, the double bond significantly decreases the freezing temperature of the adsorption layer. For example, the melting temperature is ≈ 30°C for saturated alkane with 18 C-atoms, whereas for 9-octadecen it is by 60 degrees lower, viz. around -30°C.

In the experiments with systems which do show drop deformations prior to drop freezing, we observed that the drop shape evolution was more pronounced when the surfactant was with longer tail when compared to the alkane chain length and larger differences led to more pronounced deformations (larger aspect ratio, *AR*, and deeper along the evolutionary path).

### 3.4 Effect of the cooling rate

Our experiments with a given system (alkane, surfactant, drop size) showed that the drop shape deformations proceeded further along the evolutionary scheme and, respectively, higher aspect ratios were observed when the samples were cooled at lower rates. This effect is demonstrated in Figure 28 in the Thesis. For a given system, the cooling rate changed only the temperature at which the drops freeze (with higher cooling rates, the supercooling before freezing was bigger), but it did not change the temperature at which the drop shape deformations began or the sequence of the observed drop shapes.

### 3.5 Effect of the initial drop size

The described evolutionary path was observed with all drops with sizes varied between ca. 1 and 100 μm when the experiments were performed at sufficiently slow cooling rate (< 0.1°C/min). The experimental results showed that smaller droplets deformed easier, as compared to the larger drops. For example, 16 and 31 μm drops, dispersed in $C_{18}SorbEO_{20}$ aqueous solution, reached the hexagonal prism stage before freezing at a cooling rate of 0.44°C/min, while smaller droplets (7 and 10 μm) deformed into long thin fibers at the same cooling rate, Figure 29a. To observe further deformations of the 16 μm drops, cooling rate of 0.16°C/min was needed, Figure 29b. In the same trend, for deformation of the even bigger 31 μm drops to the latest stages of the evolutionary scheme, a lower cooling rate by another order of magnitude was required.

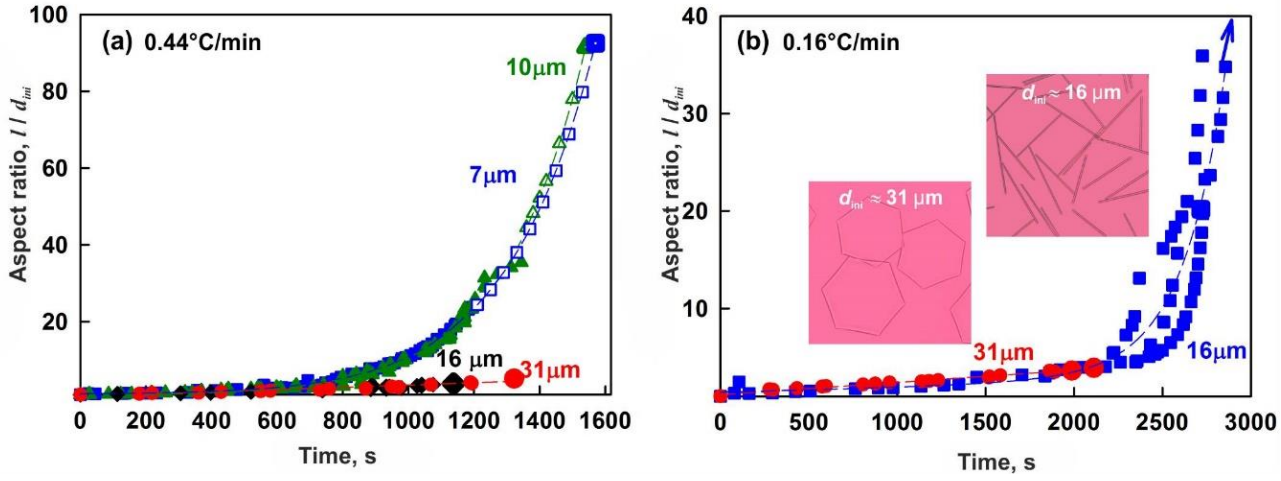


**Figure 29.** (a) Deformations of droplets of $C_{16}$ in $C_{18}SorbEO_{20}$, cooled at 0.44°C/min cooling rate. The drops have different initial drop diameters, as shown in the figure. Smaller droplets evolve easily, reaching the last stages of the evolutionary scheme, whereas the bigger droplets freeze at the hexagonal platelet stage, at significantly lower aspect ratio. (b) Deformations of $C_{16}$ in $C_{18}SorbEO_{20}$, cooled at 0.16°C/min cooling rate. The inset microscopy images show deformed droplets of different initial drop size.

### 3.6 Effect of the surfactant head group

#### *3.6.1 Nonionic surfactants with 20 ethoxy units in the hydrophilic head*

To describe the effect of the surfactant head group on the observed deformations, first, we compare the behavior of hexadecane droplets, dispersed in aqueous solutions of two different nonionic surfactants with the same hydrophobic tail and equal number of ethoxy units in the hydrophilic heads, $C_{16}EO_{20}$ and $C_{16}SorbEO_{20}$. However, all ethoxy units in $C_{16}EO_{20}$ molecule are consecutively connected to each other, while in $C_{16}SorbEO_{20}$ they form four fragments of ethylene oxide units, connected to the sorbitan ring.

The drop deformations for these systems, as a function of the temperature, at cooling rate of 0.16°C/min, are presented in Figure 30a. One sees significant differences in the behavior of the two samples – the final deformations are very different, as well as the temperatures at which the deformations begin and the temperature ranges in which deformations are observed prior to the final drop freezing. For $C_{16}/C_{16}EO_{20}$ system, the drop shape deformations start at $T_d \approx 10.5$°C and proceed in a very narrow temperature range of 2 to 3 °C, while the reached aspect ratio is much higher ($AR = 90 \pm 10$) than that observed for $C_{16}/C_{16}SorbEO_{20}$ system ($AR = 5 \pm 1$).

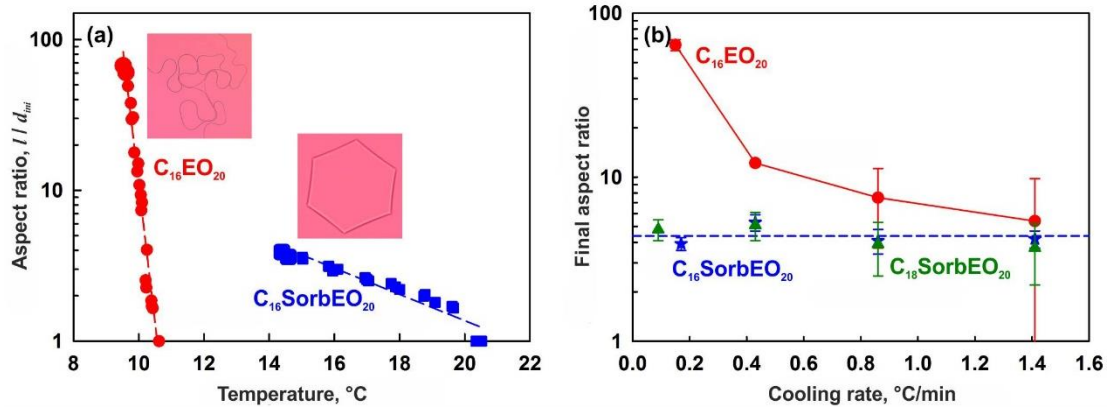


**Figure 30.** (a) Aspect ratio and (b) final aspect ratio in the moment just before drop freezing for $C_{16}$ drops with initial drop size $d_{ini} \approx 31 \pm 3$ μm, dispersed in different nonionic surfactants. Experiments in (a) are performed with cooling rate of 0.16 °C/min.

#### *3.6.2 Role of the hydrophilic head-group size for $C_nEO_m$ nonionic surfactants*

Comparison of different surfactants with formula $C_nEO_m$ showed that the differences described in section 3.6.1 are not caused by the specific presence of sorbitan ring in the head group of $C_{16}SorbEO_{20}$. The main trends observed in the process of drop shape deformations upon cooling can be summarized as follows. The general drop shape evolutionary scheme does not depend on the specific surfactant used. The various surfactants change mainly the temperature at which the deformations start and the ability of the drops to reach the last stages of the evolutionary sequence.

### 3.7 Classification of surfactants

From all performed experiments, we concluded that we could classify the studied surfactants into four categories (denoted as groups *A* to *D*), depending on their effect on the drop shape deformations, observed with hexadecane drops ($d_{ini} \approx 30$ μm), see Table 9. Similar classification could be made also for the other hydrophobic phases. However, the specific surfactants falling in one group for $C_{16}$ could fall into another group for different oil, because the difference in the lengths of the alkane molecule and the surfactant tail is very important for the observed trends.

### 3.8 Main results in Chapter III

From the performed systematic experiments we can conclude that:

(1) Spontaneous deformations of emulsion drops upon cooling are observed not only with alkanes, but also with other hydrophobic substances which pass through plastic rotator phases upon cooling, for example, *n*-alcohols, 1-alkenes, triacylglycerols and others.

(2) General evolutionary scheme is observed with all systems tested (surfactant/oil combinations). Depending on the specific system, one or another shape may be prevailing.

(3) The temperature, at which the drop shape deformations begin, depends on the specific system. Three types of systems were observed: In the first type, the drop shape deformations begin at temperature $T_d$ which is by 3-4°C higher than the bulk melting temperature of the dispersed oil, $T_m$. In the second type, the drop deformations start at $T_d \approx T_m$. In the third type, the drop shape deformations start after very significant supercooling (by 4-8°C) below $T_m$.

(4) Drop shape deformations are more pronounced for smaller droplets, which are cooled at lower rates, and are stabilized by surfactants with longer hydrophobic tails (similar or longer than the chain length of the dispersed oil). Under such conditions, the cooled drops reach larger aspect ratios along the evolution sequence before their freezing.

(5) Surfactants stabilizing the emulsions have three main effects on the observed drop deformations: (a) they change the temperature at which the drop shape deformations begin, $T_d$; (b) they change the final drop shape at which the drops freeze, and (c) they determine the ability of the drops to deform into rod-like particles and thin fibers, extruded from the acute angles of the deformed platelets or from the ellipsoidal droplets.

**Table 9.** Classification of surfactants with respect to their effect on the spontaneous drop shape deformations observed upon cooling. The classification here is for hexadecane droplets with initial diameter ≈ 32 μm. For more detailed explanations, see the text.

| | **Surfactans in the group** | **Main structural characteristic of molecules** | **Temperature of drop deformation, $T_d$, and freezing, $T_f$** | **Preferred shapes** | **Interfacial layers' strength (thickness)** |
|---|---|---|---|---|---|
| ***Group A*** | $C_{16}EO_{10}$<br>$C_{18}EO_{10}$<br>$C_{18}EO_{20}$<br><br>$C_{18}SO_4Na$ | Long tail and/or shorter EO chain<br><br>Long tail anionic | $\boldsymbol{T_d > T_m}$<br>$T_d \approx 19.5 \div 23°C$<br>$T_f \approx 10 \div 15°C$ | Fibers with diameter ≈ 1.5 μm and ≤ 0.5 μm<br>Different platelets and ellipsoidal drops extruding such fibers | Thin flexible layers |
| ***Group B*** | $C_{16}SorbEO_{20}$<br>$C_{18}SorbEO_{20}$<br>$C_{16}EO_2$ | Sorbitan ring<br><br>Short EO chain | $\boldsymbol{T_d \approx T_m}$<br>$T_d \approx 17 \div 19°C$<br>$T_f \approx 12 \div 13°C$ | Hexagonal platelets<br>Rods with diameter ≈ 5 μm<br>The platelets do not extrude asperities from their corners | Very strong (thick) layers |
| ***Group C*** | $C_{16}EO_{20}$<br>$C_{16\text{-}18}EO_{25}$<br><br>CTAB | Larger EO head and/or shorter tail ($C_{16}$)<br><br>Lang tail cationic | $\boldsymbol{T_d < T_m}$<br>$T_d \approx 10 \div 11°C$<br>$T_f \approx 8 \div 9°C$ (nonionic)<br>$T_d \approx 14.5°C$ , $T_f \approx 12.5°C$ | All shapes are observed with a transition from rods with diameter ≈ 5 μm into fibers with diameter < 1 μm | Intermediate<br>(soft rods) |
| ***Group D*** | $C_{12}$ tail<br><br>$C_{20\text{-}40}EO_{40}$<br>$C_{16}EO_{50}$<br><br>$C_{18:1}SorbEO_{20}$ | Short tail<br><br>Very large head-group<br><br>Double bond in the tail | $\boldsymbol{T_d}$ **– not observed**<br>$T_f \approx 5 \div 8°C$ for short tails<br>$T_f \approx 9 \div 13°C$ for large heads | Spherical | - |

# Chapter IV. Mechanism of spontaneous deformations

Drop shape deformations upon cooling are accompanied with significant increase of the interfacial area between the oil and surfactant solution and, respectively, with an increase of the oil-water interfacial energy. Despite that, the observed deformations are spontaneous, which means that they correspond to decreasing overall energy of the emulsion system. Therefore, the mechanism of these deformations should be clarified in more detail.

## 4.1 Type of information obtained from each experimental method

To check the possible hypothesis that the drop deformations are possible because the oil-water interface has an ultra-low interfacial tension and, hence, the increase of the interfacial area does not increase significantly the interfacial energy of the system, we performed interfacial tension measurement. Differential scanning calorimetry (DSC) measurements allowed us to determine the enthalpy released upon drop shape deformation before freezing, and small angle X-ray scattering (SAXS) gave us direct information about the arrangement of the molecules within the deformed droplets. The results from all these measurements were compared to the processes observed by optical microscopy using the same cooling/heating protocol.

## 4.2 Control experiments

To test whether our system does not contain surface active contaminants, we measured the interfacial tension of purified hexadecane drops, immersed in pure deionized water. The measured value was $52 \pm 0.5$ mN/m and remained constant for a period of $> 15$ min which shows that the system was with high purity.

The control DSC experiments included measurements of the thermal signal, obtained upon cooling of various surfactant solutions used for emulsification (without oil included in these control experiments). In these samples we did not detect any measurable peaks in the relevant temperature range. In separate experiments, we tested dodecane emulsion, stabilized by long chain surfactant at experiments in which drop deformation and drop freezing are not observed. In these experiments, we also did not observe any measurable peaks in the thermograms. All these results show that the peaks in the thermograms presented in the following sections are entirely due to changes in the dispersed oily phase.

To check that the signal in SAXS experiments is also entirely due to changes in the oily drops, we measured the signal obtained upon cooling of the surfactant solutions, without added oil. No measurable peaks were detected in these control experiments either.

In sections 4.3 to 4.6 we present our experimental results for various alkane/surfactant systems, following the classification presented in Table 9.

### 4.3 *Group D*: systems without deformations

Surfactants that do not induce drop deformations prior to drop freezing belong to *Group D* is our classification. Surfactants in this group have short hydrophobic tail or large hydrophilic head group. In these systems, rotator phase formation prior to drop freezing (crystallization) is not expected.

Interfacial tension measurements, as a function of the temperature, were performed for $C_{16}/C_{16\text{-}18}EO_{50}$ system. The measured IFT was relatively high, about 16 to 17.5 mN/m and slightly increased upon cooling, following the typical $\gamma(T)$ dependence, see Figure 36 in the Thesis.

Optical and DSC experiments were also performed with several systems belonging to *Group D*. DSC thermogram obtained with hexadecane drops, dispersed in $C_{16\text{-}18}EO_{50}$ surfactant solution, is shown in Figure 37. As seen from the DSC curve, we observe one main peak with Gaussian shape, centered around $T \approx 6$°C, and two small peaks around 15°C. From the performed optical observations we saw that the peak with maximum at 6°C forms due to the complete crystallization of the dispersed emulsion droplets, whereas the peaks at 15°C are due to the freezing of single much larger in size emulsion droplets and some oil lenses formed on the surface of the emulsion sample as a result of drop coalescence either with other drops or with the emulsion-air interface (i.e. these last peaks are artifacts). It is very important to note that in **neither** of the systems studied from *Groups A, B* or *C* we did not observe any big drops or oil lenses. The coalescence of the original droplets was suppressed in these latter systems as the adsorption layer was sufficiently dense to protect the drops.

In SAXS experiments with $C_{16}/C_{12}SorbEO_{20}$ sample belonging to *Group D*, Figure 39 in Thesis, we detected a single peak, which appeared at $T \approx 9$°C with maximum at scattering vector $q \approx 3.05$ nm$^{-1}$. This peak increased its intensity with the temperature decrease, reaching a maximal intensity around 6°C. This value of the scattering vector corresponds to formation of lamellar phase with thickness $h \approx 2.06$ nm, which is equal to the typical thickness for the triclinic hexadecane crystal structure.[103] At scattering vector $q \approx 2.8$ nm$^{-1}$ which is the typical value for the rotator phase of hexadecane we did not observe any measurable peak in this system. From the obtained results we can conclude that the drops in the system $C_{16}/C_{12}SorbEO_{20}$ crystallize directly into the triclinic phase without passing through any intermediate rotator phase.

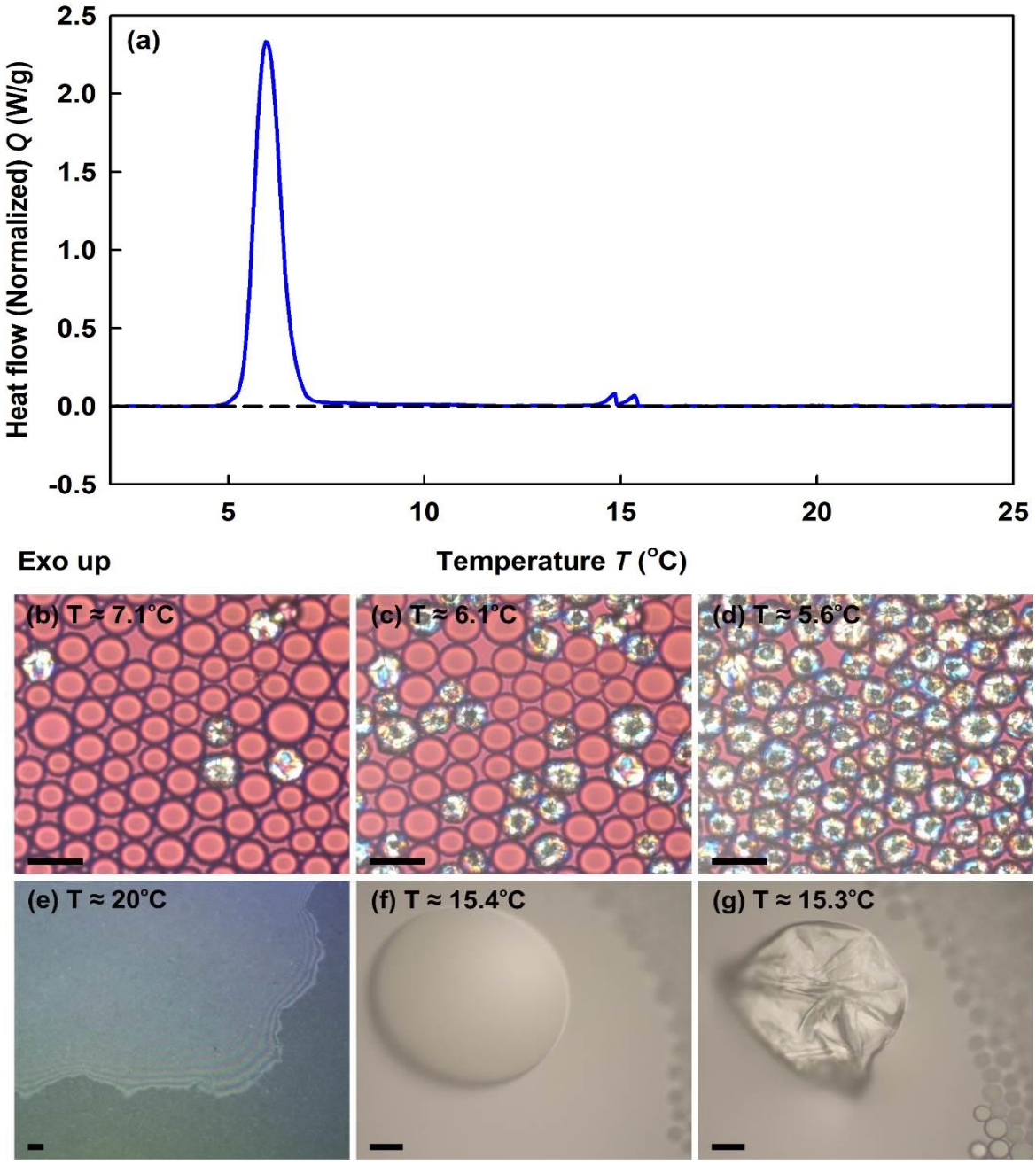


**Figure 37. DSC thermogram and microscopy images for $C_{16}$ drops with initial drop size, $d_{ini}$ ≈ 10 µm, stabilized by $C_{16\text{-}18}EO_{50}$ surfactant (*Group D*).** (a) DSC thermogram upon cooling; (b-d) Microscopy images in transmitted polarized light, showing the process of drop freezing upon cooling. The cooling experiment is performed in glass capillary. (b) The first freezing process is observed at temperature 9.3ºC, however, as seen in this picture, only a very small fraction of the drops has frozen down to 7.1ºC. (c-d) The main freezing process is observed between 6.5ºC and 5.6ºC. (e-f) Cooling experiment of the same sample, contained in a DSC pan. The drops are observed in reflected white light. The small peaks, observed in the thermogram around 15ºC are due to freezing of oil lenses and some very large drops, formed after drop-drop coalescence. (e) Oil lenses are observed at the top of the sample, placed in a DSC pan. (f) Fluid big drop. (g) The drop freezes at a temperature 15.3ºC. All experiments (both DSC and optical observations) are performed at 0.5°C/min cooling rate. Scale bars, 20 µm.

### 4.4 Group B: systems for which the deformations start at $T_d \approx T_m$

The systems $C_{16}/C_{16}SorbEO_{20}$ and $C_{16}/C_{18}SorbEO_{20}$ belong to *Group B* in our classification, Table 9, and were used in the following model experiments.

Interfacial tension measurements for these systems showed that it was between 5.5 and 7.5 mN/m at temperatures, at which the drop shape deformations started.

In the DSC experiments with samples from *Group B*, we observed peaks at temperatures at which the drop shape deformations have begun while the drops were still in fluid state (not frozen yet). An illustrative thermogram from such measurements is presented in Figure 41. For this specific system we did not observe any drop crystallization down to temperature around 12°C – neither in the capillary experiments nor in the DSC pan experiments. This means that the peaks observed at $T > 12$°C are entirely due to enthalpy released in the process of molecular rearrangement of the hexadecane in the fluid oil drops (with a possible contribution from the freezing surfactant adsorption layer). The peaks detected at $T < 12$°C are caused by a combination of the continuous drop shape deformations and the final drop freezing.

From four independent measurements, we determined that the enthalpy released between the beginning of the drop deformations down to 12.2°C is 3.8 ± 0.6 % from the total enthalpy measured in the whole DSC experiment. This means that ≈ 3.8% of the total enthalpy has been released along the transition from isotropic liquid phase into a phase with higher order, before any freezing (crystallization) of the oily drops is observed.

From these measurements we are able to determine the thickness of the plastic rotator phase formed on the tetragonal particle surface as explained in Chapter V. Depending on the specific model adopted in these calculations, we estimate the thickness of the ordered phase to be around 55 nm ± 15 nm which corresponds to 24 ± 6 layers of ordered molecules.

In a separate series of experiments, we studied the behavior of $C_{16}/C_{16}SorbEO_{20}$ drops with initial diameter $d_{ini} \approx 3$ μm. For this system, we also detected peaks at high temperatures prior to any drop freezing. The enthalpy released in the system from the beginning of the drop shape deformations down to 13.8°C, where the main fraction of the droplets have adopted rod-like shape with length ≈ 15.2 ± 2.3 μm, was around 2.7 ± 0.8 % from the total enthalpy released in the whole experiment (average value from 10 independent experiments) – these results were also used to estimate the thickness of the layer of rotator phase on the drop surface, as explained in Chapter V.

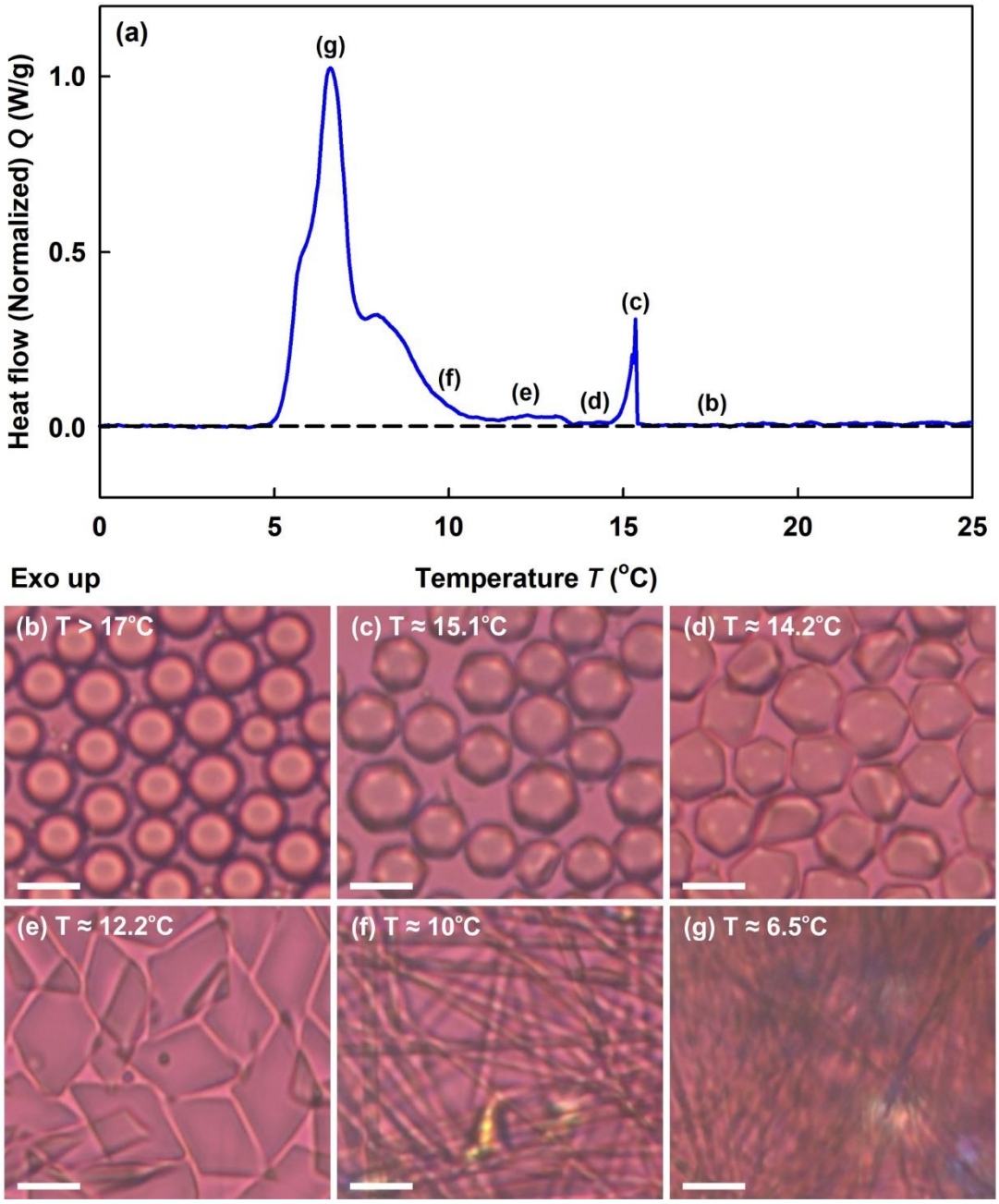


**<u>Фигура 41.</u> DSC thermogram and microscopy images for $C_{16}$ drops with $d_{ini} \approx 9.5 \pm 0.1$ μm, stabilized by $C_{16}SorbEO_{20}$ surfactant (*Group B*).** (a) DSC thermogram, obtained at 0.5 °C/min cooling rate; (b-g) Microscopy images showing the consequtive stages of the drop shape evolution upon cooling; cooling rate 0.5 °C/min. (b) All emulsion drops are spherical at temperatures above 17ºC. (c) Drop shape transformations start around 15.2 ± 0.2ºC (data from 4 independent measurements), for this particular sample the peak starts at 15.4ºC. At this temperature, the DSC curve starts to deviate from the baseline. (d) At temperature around 14.2ºC flattened polyhedrons are formed. (e) The decrease of the temperature leads to further evolution in the drop shape. At temperature around 12.2ºC, the drops have evolved up to the stage of tetragonal platelets. (f) Some rare drops were observed to freeze at 11ºC ≤ $T$ ≤ 12ºC, while most of the drops elongate into long fibers. (g) The thin elongated fibers freeze (crystallize) completely at $T \approx 6.5$ºC. Scale bars, 10 μm.

To obtain direct structural data for the arrangement of the molecules inside the non-spherical drops, we performed SAXS measurements with $C_{16}/C_{16}SorbEO_{20}$ emulsion containing drops of size $d_{ini} \approx 13$ μm. In these measurements we observed diffraction peaks at similar temperatures as those at which DSC peaks were observed, i.e. when the drop shape deformations began. Initially, we expected to see only rotator phase peak at high temperatures. Surprisingly, the experimental results showed almost simultaneous formation of rotator phase peak ($q \approx 2.82$ nm$^{-1}$) and a second peak of similar area with maximum at $q \approx 3.05$ nm$^{-1}$. Both peaks increased their intensity upon cooling and they had identical areas at around $T \approx 12$°C. Upon additional cooling, the rotator phase peak started to decrease its intensity, while the peak at 3.05 nm$^{-1}$ increased intensity. At the end, when all particles froze, a single peak with maximum around 3.05 nm$^{-1}$ was observed, Figure 43a.

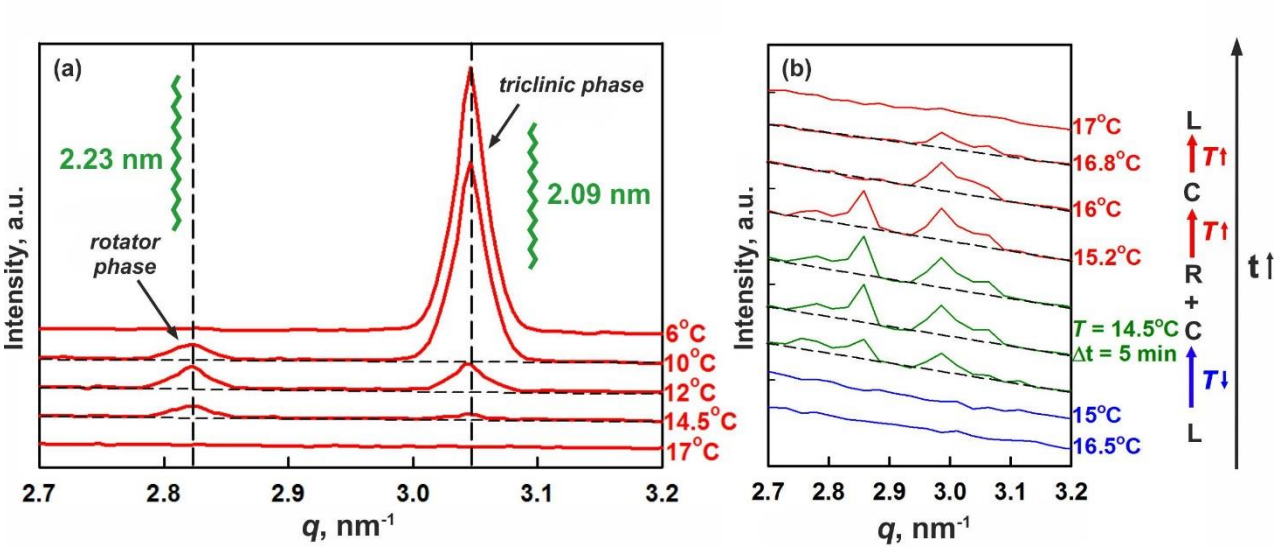


**Figure 43. SAXS results obtained with the system $C_{16}/C_{16}SorbEO_{20}$.** The initial drop diameter is ≈ 13 μm. (a) Signal obtained in experiment at constant cooling rate of 0.5°C/min. The initial peaks are observed at $T \approx 14.5$°C. These peaks show that two phases with characteristic periods of 2.23 nm and 2.09 nm form in the sample. The rotator phase peak disappears after the complete sample freezing (at $T \approx 6$°C). (b) Signal obtained upon cooling with constant cooling rate down to $T \approx$ 14.5°C. When this temperature was reached, it was hold constant for 10 minutes and, afterwards, the sample was heated. Both peaks disappeared at 17°C. See text for more explanations.

To make sure that these results show the co-existence of two surface phases – one with characteristics of the rotator phase and the second one – with the characteristics of the triclinic crystalline phase in a certain temperature range, we performed additional experiments. The other possible explanation could be that the observed crystalline peak is due to freezing of some of the droplets inside the sample, whereas the rotator phase peak is caused by the deformations of the remaining droplets. To rule out the latter possibility in our additional experiments we decreased the temperature in the sample down to 14.5°C and then held the temperature constant for 10 min, the

green curves in Figure 43b. Afterwards, we increased the temperature in the sample stepwise and hold it constant for a few minutes at the different temperatures, the red curves in Figure 43b. Upon this temperature increase, we observed that the rotator phase peak disappeared at temperature around 16°C, and then upon further heating, the peak of the "crystalline phase" also disappeared completely at 17°C. The latter result shows directly that the crystalline peak is not caused by the bulk freezing of some drops in the sample - it is indeed due to the co-existence of thin ordered layers of alkane molecules structured in phases with characteristics of rotator and crystalline phase (otherwise, the crystalline peak would disappear at $T_m$ = 18°C).

On the basis of these results, we could refine the mechanism of drop shape deformations for this system as follows (Figure 44): Initially, both alkane molecules inside the drops and the adsorption layer are in a liquid state. Upon cooling, the surfactant adsorption layer freezes and it induces the ordering of the alkane molecules next to the drop surface. The molecules closest to the surface arrange in layers with structural characteristics similar to those of the crystallized alkane molecules. The molecules in the inner layers, however, arrange in rotator phase as their ordering is disrupted due to the decreasing number of molecules in the inner layers, caused by the surface curvature.

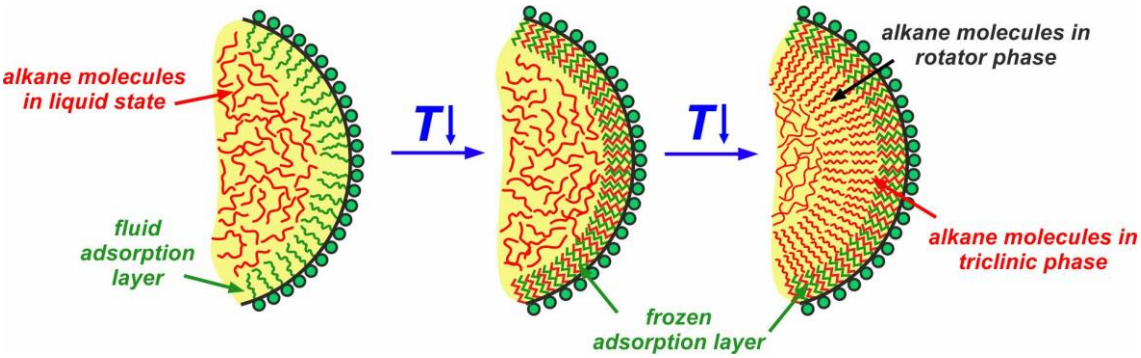


**Figure 44. Schematics of the drop shape deformation mechanism.** See text for more details.

### 4.5 *Group C*: systems for which the deformations start at $T_d < T_m$

The DSC measurements with the emulsion $C_{16}/C_{16}EO_{20}$ containing drops with $d_{ini} \approx 2.6$ μm showed appearance of the first peak in the thermograms at similar temperatures as the temperatures at which the drop shape deformations began. However, fraction of the drops (≈ 8 ± 2%) in this system froze soon after the initial deformations, at $T \approx 10$°C. The rest of the drops deformed into elongated thin fibers and froze at significantly lower temperatures around 5°C. The observed drop freezing makes the quantitative data interpretation somewhat more subtle, but still possible.

In the thermograms for this system we observed deviation of the signal from the baseline at $T \approx$ 10.5°C followed by wide "tail" of this first peak down to around 6.5°C, where a second peak started. The Gaussian peak at low temperatures is caused by the final freezing (crystallization) of

the deformed drops. From five independent measurements, we determined that the enthalpy released in the first peak is ≈ 16.5 ± 1.2 % of the total enthalpy released upon sample freezing, while the second peak enthalpy was ≈ 83.5 %.

The enthalpy of the first peak is ≈ 2 times larger than that originating from the drops frozen (crystallized) at this stage. Therefore, we concluded that about half of the first peak is due to the enthalpy released around 10°C in the process of drop deformation without alkane freezing. This interpretation is supported also by the fact that the first peak in the thermograms is observed throughout a wide temperature range, between 10.5 and 6.5°C, whereas no any further drop freezing was observed between 10 and 6.5°C after the initial freezing at around 10°C. This means that the DSC signal observed between 10 and 6.5°C is entirely associated with the drop shape transformations in this temperature range.

From the measured enthalpy, under the assumption that the rotator phase forms only on the cylindrical rods surface, see section 5.2 in Chapter V, we calculated that the thickness of the rotator phase in this case is around 8 ± 2 nm, i.e. 3 ± 1 consecutive layers of ordered molecules.

### 4.6 *Group A*: systems for which the deformations start at $T_d < T_m$

In the interfacial tension measurements with systems from *Group A* we were able to detect directly the process of surface freezing, see Figure 47 in Thesis. The temperature of surface freezing, however, did not correspond to the temperature at which the drop shape deformations were observed. This is most probably caused by the fact that the millimeter sized droplets, used in the IFT measurements, have much lower curvature when compared to the micrometer droplets used in the emulsion experiments. Therefore the conditions for surface freezing can be different, as the temperature of surface freezing may depend on surface curvature. Nevertheless, the values of the measured interfacial tension always were in the range between 4 and 6 mN/m at the temperatures, at which we observed the beginning of drop shape deformations (far higher than "ultra-low" interfacial tension).

In the DSC measurements for the system $C_{16}/C_{16}EO_{10}$ with drops with initial diameter $d_{ini} \approx 33$ μm, we detected a small, but well reproducible peak at $T \approx 21 – 21.5$°C. At the same temperature we observed the beginning of the shape deformations of the dispersed drops in the microscopy experiments. At temperatures below this peak we observed continuous exothermic deviation of the DSC curve above the baseline, which reflected the continuous drop shape transformations in this temperature range. This behavior was explained with the specific deformations observed in this system – these drops deformed into polyhedrons with irregular shapes and corrugated surface, and several subsequent breakage events into smaller drops were observed upon cooling.

The estimate of the rotator phase thickness for this system is discussed in section 5.3 in chapter V. The final results depended very much on the assumptions made. If we assume that the rotator phase forms on the entire drop surface with uniform thickness, then we estimate the thickness of the plastic rotator phase to be around 5-6.25 nm (viz. 2-3 layers of molecules). Alternatively, if we assume that the rotator phase is formed not as a homogeneous layer on the entire surface of the polyhedral drops, but on the edges of the polyhedrons only (assumption which corresponds much better to our explanation for the origin of the drop shape transformations), then we estimate that the rotator phase has much larger thickness, between ca. 30 and 180 nm.

### 4.7 Main results in Chapter IV

The following main conclusions can be made from the experiments performed to understand the mechanism of drop-shape deformations upon cooling:

(1) The values of the interfacial tension measured at the temperatures, at which the drop shape deformations begin, varies between 4 and 8 mN/m. Therefore, the observed drop-shape evolution cannot be explained with ultra-low interfacial tensions. Hence, the surface energy of the system increases along the drop-shape transformations.

(2) In the performed DSC experiments, we detected peaks prior to drop freezing for all systems in which drop shape deformations were observed. These peaks appeared at temperatures close to the temperature at which the drop shape deformations began. These peaks could be explained only if one assumes that thin layers of plastic rotator phase are formed next to the drop surface.

(3) Formation of ordered phase prior to any drop freezing was detected directly in the experiments with $C_{16}/C_{16}SorbEO_{20}$ system by SAXS. The formed intermediate phase combines structural characteristics of both rotator and crystalline phases, i.e. there is coexistence between thin layers of these two phases. This result allowed us to refine (for this system) the initially proposed mechanism of drop deformations as follows: Upon cooling, the adsorption layer freezes and induces ordering of the alkane molecules next to the drop surface in a thin layer of phase with characteristics similar to those of the triclinic crystalline phase. The surface curvature, however, disrupts the regular molecular ordering and leads to the accumulation of defects in the inner ordered layers. Therefore, the molecules in these inner layers arrange in a phase with characteristics of the rotator phase.

# Chapter V. Theoretical interpretation of the results

In this chapter, we present the theoretical models, developed to estimate the thickness of the plastic rotator phase which is formed on the surface of the various non-spherical drops using the data from the DSC and SAXS experiments.

## 5.1 Estimate of the thickness of the plastic rotator phase in tetragonal platelets

### *5.1.1 Calculation of the volume of tetragonal platelets*

To estimate the thickness of the rotator phase formed on the surface of tetragonal platelets, we need to calculate their surface area and to model adequately their shape. From the optical observations, we modeled the tri-dimensional shape of the tetragonal drops as thin tetragonal prism with height $h_m$ which is surrounded by a cylindrical frame with radius of curvature $r$, see Figure 51b.

We derived the following equation for the volume of the tetragonal drops, as a function of the side lengths of the two-dimensional particle projection, $a$ and $b$, and the acute angle between these sides, α (which we can directly measure from the experiment), and also of the parameters $h_m$ and $r$ which we do not know with high precision:

$$V_{particle} = V_{ini} = \frac{1}{6}\pi d_{ini}^3 = \pi r^2\left(2a+2b-\frac{8r}{\sin\alpha}\right)+h_m\sin\alpha\left(a-\frac{4r}{\sin\alpha}\right)\left(b-\frac{4r}{\sin\alpha}\right)+ \\ +\left(\frac{h_m}{2}\left(2r-\sqrt{r^2-\frac{h_m^{\,2}}{4}}\right)-r^2\arcsin\frac{h_m}{2r}\right)\left(2a+2b-\frac{16r}{\sin\alpha}\right) \qquad (11)$$

### *5.1.2 Calculation of the rotator phase thickness*

To calculate the rotator phase thickness we need to derive an additional equation which connects the geometrical parameters that can be measured directly in the optical observations ($a$, $b$ and α) to the volume of the rotator phase which is measured in the DSC experiments.

We adopted two alternative models, Figure 51. In the first model (upper limit estimate) we assumed that the rotator phase is formed only at the external surface of the cylindrical frame, in the regions of the surface which have high curvature, see Figure 51c. In the second model we assumed that the rotator phase is formed with homogeneous thickness on the entire particle surface, Figure 51d. Our experimental results show that *Model I* corresponds better to the observed drop behavior.

***(a) Model I – upper limit estimate***

The final expression which allows us to calculate the thickness of the plastic rotator phase, according to *Model I*, is:

$$V_{rot\ ph}^{I} = \left(2a + 2b - \frac{8r}{\sin\alpha}\right)\left(2\pi r h_{PL} - \pi {h_{PL}}^2\right) - \left(2a + 2b - \frac{16r}{\sin\alpha}\right) \times$$
$$\times \left( \frac{h_m}{2}\left( \sqrt{r^2 - \frac{{h_m}^2}{4}} - \sqrt{\left(r - h_{PL}\right)^2 - \frac{{h_m}^2}{4}} \right) + r^2 \arcsin\frac{h_m}{2r} - \left(r - h_{PL}\right)^2 \arcsin\frac{h_m}{2\left(r - h_{PL}\right)} \right) \quad (14)$$

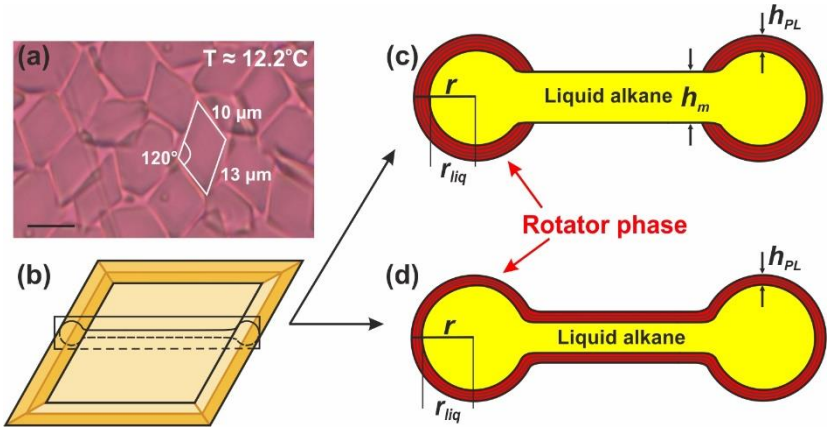


**<u>Figure 51.</u> Calculation of the rotator phase thickness for tetragonal platelets (*Group B*).** (a) Microscopy image of fluid tetragonal platelets, obtained upon cooling of $C_{16}$ emulsion sample stabilized by $C_{16}SorbEO_{20}$ surfactant. The initial drop size is $d_{ini} \approx 9.5$ µm, drops are cooled at 0.5 °C/min (see section 4.4 for more detailed explanation of the experiment). Scale bar, 10 µm; (b) Sketch of a fluid platelet; (c-d) Sketches of the two alternative models used to estimate the thickness of the rotator phase, formed at the platelet surface: (c) *Model I*: Geometrical model in which we assume that the rotator phase is formed only at the platelet periphery (in the regions of high interfacial curvature) while the alkane in the inner part of the drop is in a liquid state; (d) *Model II*: Geometrical model assuming that a homogeneous layer of rotator phase is formed over the entire surface of the deformed drop. See text for more details.

***(b) Model II – lower limit estimate***

The final expression for the volume of rotator phase, calculated according to *Model II* is:

$$V_{rot\ ph}^{II} = V_{rot\ ph}^{I} + 2h\sin\alpha\left(a - \frac{4r}{\sin\alpha}\right)\left(b - \frac{4r}{\sin\alpha}\right) + 2h_{PL}\left(r - \sqrt{r^2 - \frac{{h_m}^2}{4}}\right)\left(2a + 2b - \frac{16r}{\sin\alpha}\right) \quad (17)$$

Equations (14) and (17) were used to estimate the thickness of the rotator phase, $h_{PL}$, in *Model I* and *Model II*, respectively. Assuming a certain ratio for the thickness of the middle plate over the cylinder radius, $h_m/r$, we determined the value of $h_{PL}$ which satisfies eq. (14) or eq. (17) (depending on the model used), while satisfying equation 11 as well. Thus we evaluated the range of possible variations of $h_{PL}$ for the entire reasonable range of $h_m/r$ ratios, varied between 0.2 (very thin central part of the platelet) and 1.9 (central part almost equal in thickness to the cylinder diameter).

### *5.1.3 Interpretation of the experimental results*

Using the main geometric parameters for the tetragonal drops formed in the system $C_{16}/C_{16}SorbEO_{20}$ at 12.2°C, as well as the enthalpy measured from the beginning of the drop shape deformations down to 12.2°C, we estimated the following thicknesses of the surface layer of rotator phase:

Using *Model I*, we found $h_{PL} \approx 49 \pm 5$ nm for $h_m = 0.2r$ and $70 \pm 5$ nm for $h_m = 1.9r$. Thus, we see that the most probable value of $h_{PL}$ is around $55 \pm 15$ nm, which corresponds to a multilayer of $\approx 24 \pm 6$ parallel layers of ordered hexadecane molecules.

Using *Model II* (homogeneous rotator phase on the entire drop surface), we calculated $h_{PL} \approx 40 \pm 7$ nm for $h_m = 0.2r$ and $51 \pm 6$ nm for $h_m = 1.9r$. Thus, we see that the most probable value of $h_{PL}$ in this model is $45 \pm 13$ nm, viz. $20 \pm 6$ ordered layers.

## 5.2 Estimate of the thickness of the plastic rotator phase, formed in rod-like drops

### *5.2.1 Geometrical model*

The rod-like drops have cylindrical shape. Therefore, we assumed that rotator phase with homogenous thickness is formed on the surface of the cylinder only, whereas the inner alkane molecules remain in liquid state, thus forming an inner cylinder with radius $r_{liq}$, filled with liquid alkane, Figure 53 in Thesis. This assumption is supported by the observation that the thin cylindrical drops significantly increase their length upon cooling, keeping at the same time their elastic properties.

The volume of the inner cylinder, filled with liquid phase, is $V_{liq} \approx \pi r_{liq}^2 L$, while the rotator phase volume is $V_{PL} \approx \pi\left(r^2 - r_{liq}^2\right)L$, where $r$ is the radius of the whole cylinder, $r_{liq}$ is the radius of the inner cylinder, and $L$ is the cylinder length.

### *5.2.2 Interpretation of the experimental results*

Using the model described above, we estimated the thickness of the rotator phase layer for two systems in which the drops deform into rod-like shapes. For the system $C_{16}/C_{16}SorbEO_{20}$ and drops with initial size $d_{ini} \approx 3$ μm, Figure 42 in Thesis, we found that the plastic phase thickness is $9.4 \pm 3$ nm, i.e. this is a multilayer with $4 \pm 1$ ordered layers of alkane molecules. For the system $C_{16}/C_{16}EO_{20}$ ($d_{ini} \approx 2.6$ μm, Figure 46 in Thesis), we calculated $h_{PL} \approx 8 \pm 2$ nm ($3 \pm 1$ layers of molecules).

### 5.3 Estimate of the thickness of the plastic phase, formed in systems from *Group A*

Under the assumption that a thin layer of rotator phase is formed with uniform thickness on the entire drop surface, we calculated 6.25 nm ≥ $h_{PL}$ ≥ 5.00 nm (2-3 layers of molecules) for $C_{16}/C_{16}EO_{10}$ system. In the alternative model, in which the ordered phase forms only on the edges of the non-spherical drops, we calculated a layer thickness in the range between 30 and 180 nm, depending on the specific assumptions made. These results show that multilayers of plastic rotator phase are formed also in this system belonging to *Group A.*

### 5.4 Thickness and mechanical strength of the layers of rotator phase

In our experiments we observed characteristic curvature with radius of the order of $r \approx 1$ μm at the edges of the shaped drops. For such non-spherical shapes to exist at finite interfacial tension, γ, the capillary pressure should be overcome mechanically – otherwise, the drops would stay spherical to minimize their surface energy. The balance of the bending moments created by the interfacial tension and the plastic rotator phase requires that the bending elasticity constant of the layer of plastic phase, formed at the surface of the shaped drops, should satisfy the relation:

$$K_B \geq \gamma r^2, \tag{19}$$

where $K_B$ is the bending elasticity constant of the interface (including the multilayers of the rotator phase) and $r$ is the radius of curvature.

Knowing the limits in which γ and $r$ vary in our systems, we calculated values for $K_B \approx 10^{-16} \div 10^{-14}$ J. However, these values are by one or two orders of magnitude higher than those reported in the literature for frozen lipid bilayers and adsorption monolayers ( $K_B \approx 10^{-18}$ J to $10^{-17}$ J )[19,20].

To estimate the thickness of the rotator phase theoretically, we need to adopt some relation between the bending elasticity constant of $K_B$ and the multilayer thickness, $h_{PL}$. Two different models are used in the literature for such lamellar multilayers – the model proposed by Evans and Skalak[19,140] and the model developed by Kirchoff and Love[141].

In his original study, Evans acknowledged that the biological membranes have non-zero shear modulus, but also suggested that the respective contribution to bending is small enough to be neglected. Under this assumption, the bending elasticity constant is proportional to the square of the plastic phase thickness, $K_B \sim h_{PL}^2$. Adopting this model, in our initial studies we estimated the rotator phase thickness to be in the range between 15 and 300 nm, depending on the specific values of the radius of curvature and interfacial tension.[10,18] However, these values seem to overestimate the thickness of the ordered phase, as determined by us in the subsequent DSC measurements and described above.

In the alternative Kirchoff-Love model[141], the extreme of bending a fully solid isotropic layer is considered and $K_B \sim h_{PL}^3$. This assumption leads to the following estimate:

$$h_{PL} \geq h_{mono} \left( \gamma r^2 / K_{B,mono} \right)^{1/3}, \quad (21)$$

where $K_{B,mono}$ is the bending elasticity modulus for a monolayer incorporated in a multilayer stack.

Taking a high estimate for $K_{B,mono} \approx 10^{-17}$ J, $h_{mono} \approx 2$ nm, and $r \approx 1$ μm, we estimate that $h_{PL}$ should be ≥ 16 nm for γ ≈ 5 mN/m and $h_{PL} \geq 7$ nm for γ ≈ 0.5 mN/m. These estimated values become twice higher if we use $K_{B,mono} \approx 10^{-18}$ J instead of $10^{-17}$ J. Thus we see that the values estimated by Kirchoff-Love model[141] are closer to those determined in our DSC experiments.

### *5.5 Main results in Chapter V*

The following main conclusions can be made from the theoretical estimates and the data interpretation performed in the current chapter:

(1) Drop shape deformations observed upon cooling are caused by formation of thin multilayers of plastic rotator phases next to the drop surface.

(2) The thickness of the layer of rotator phase in the systems of *Group B,* for which the deformations begin at $T_d \approx T_m$, depends significantly on the non-spherical shapes formed upon cooling. The calculated plastic phase thickness is $h_{PL} \approx 55 \pm 15$ nm for drops with $d_{ini} \approx 9.5$ μm deformed into tetragonal prisms. This thickness corresponds to ≈ 24 ± 6 stacked monolayers of ordered molecules. For the rod-like particles formed from 3 μm drops in the same system, the calculated rotator phase thickness is ≈ 10 nm, i.e. around 4 ± 1 layers of molecules.

(3) For systems belonging to *Group A*, $T_d > T_m$, depending on the assumption made about the rotator phase distribution on the deformed drop surface, the estimated thickness vary between 5 and 180 nm, i.e. between 2 and 80 layers of ordered alkane molecules. Additional experiments are needed to estimate the rotator phase thickness in a narrower range for this type of systems.

(4) The obtained experimental results allow us to conclude that the interlayer interactions in the plastic phase are closer to those in solid crystal structures as compared to those in the biomembranes. The measured thickness of the rotator phase is better described by the Kirchoff-Love theory of thin elastic shells, predicting $K_B \sim h_{PL}^3$, as compared to the Evans-Skalak model predicting $K_B \sim h_{PL}^2$.

## Main scientific contributions in the Thesis

1. The factors which can be used for control of the spontaneous drop deformations, observed upon emulsion cooling, are clarified. It is shown that the drops in these systems deform further along the universal evolutionary scheme when: (a) the drops have smaller initial size, (b) emulsions are stabilized by surfactants with saturated linear tail whose length is similar or larger than that of the dispersed oil molecules and/or (c) the samples are cooled at lower rates. These trends are observed with various oil-in-water emulsions, prepared with series of several *n*-alkanes, 1-alkenes, *n*-alcohols, asymmetric alkanes, and other hydrophobic substances, composed of molecules containing long saturated alkyl chains. Plastic rotator phases are known to form for all these substances, prior to their bulk crystallization.

2. The mechanism of drop shape deformations upon cooling has been clarified. It includes freezing of the surfactant adsorption layer on the drop surface, which further induces ordering of the adjacent layers of hydrophobic molecules. Via DSC and SAXS experiments we determined the percentage of alkane molecules undergoing phase transition prior to drop freezing and also the type of molecular arrangement for several of the systems.

3. A theoretical model for interpretation of the experimental data and for estimation of the rotator layer thickness has been developed. Using this model we showed that the rotator layer thickness in some of the systems is 55 ± 15 nm, i.e. 24 ± 6 stacked monolayers or ordered molecules. For other systems, the thickness corresponds to a few lengths of alkane molecules.

4. The obtained results indicate that the interactions inside the formed plastic multilayers are closer to those in solid crystals in which significant resistance exists for shearing of the neighboring layers with respect to each other. As a result, the bending elasticity constant $K_B \sim h_{PL}^3$, i.e. the properties of these layers are better described by Kirchoff-Love model, as compared to the Evans-Skalak model.

**Scientific papers included in the Thesis:**

1. D. Cholakova, N. Denkov, S. Tcholakova, I. Lesov, S. Smoukov, Control of drop shape transformations in cooled emulsions, *Adv. Colloid Interface Sci.*, **2016**, *235*, 90-107.

2. N. Denkov, D. Cholakova, S. Tcholakova, S. Smoukov, On the mechanism of drop „self-shaping" phenomenon in cooled emulsions, *Langmuir*, **2016**, *32*, 7985-7991.

3. D. Cholakova, N. Denkov, S. Tcholakova, Z. Valkova, S. Smoukov, Multilayer formation in self-shaping emulsion droplets, *Langmuir*, **2019**, *35*, 5484-5495.

**Citations of the papers included in the Thesis:**

**17 citations** of the articles included in this Thesis have been noticed:

**Paper (1) – 8 citations:**

- Hensel et al., ***Proc. Natl. Acad. Sci. U. S. A.*** **2017**; doi: 10.1073/pnas.1700099114
- Guttman et al., ***Langmuir*** **2017**, 33 pp. 1305-1314; doi: 10.1021/acs.langmuir.6b02926
- Fedoseev et al., ***Eurasian Phys. Tech. J.*** **2017**, 14 pp. 18-24.
- Cejkova et al., ***Artificial Life*** **2018**, 24; doi: 10.1162/ARTL_a_00255
- Kaptay, ***Adv. Colloid Interface Sci.*** **2018**, 256 pp.163-192 ; doi: 10.1016/j.cis.2018.04.007
- Fedoseev & Shisulin, ***Physics of the solid state*** **2018**, 60 pp. 1398-1404. doi: 10.1134/S1063783418070120
- Carpenter et al., ***Proc. Natl. Acad. Sci. U. S. A.*** **2019**; doi: 10.1073/pnas.1900802116
- Liber et al., ***Langmuir*** **2019**, 35 pp 13053-13061; doi: 10.1021/acs.langmuir.9b01833

**Paper (2) – 7 citations:**

- Zheng et al., ***ACS Nano*** **2017**, 11 pp. 721-729; doi: 10.1021/acsnano.6b07126
- Guttman et al., ***Langmuir*** **2017**, 33 pp. 1305-1314; doi: 10.1021/acs.langmuir.6b02926
- Tokiwa et al., ***Langmuir*** **2018**, 34 pp 6205–6209; doi: 10.1021/acs.langmuir.8b01088
- Zhu et al., ***Materials*** **2018**, 11, 1130; doi: 10.3390/ma11071130
- Matsubara & Aratono, ***Langmuir*** **2019**, 35, 1989-2001; doi: 10.1021/acs.langmuir.8b01203
- Marin et al., ***J. Colloid Interface Sci.*** **2019**, 538, 541-545; doi: 10.1016/j.jcis.2018.11.111
- Guttman et al., ***Nano Letters*** **2019**, 19, 3161-3168; doi: 10.1021/acs.nanolett.9b00594

**Paper (3) – 2 citations:**

- Liber et al., ***Langmuir*** **2019**, 35 pp 13053-13061; doi: 10.1021/acs.langmuir.9b01833
- Yan et al., ***Angewandte Chemie Int. Ed.*** **2020**; doi: 10.1002/anie.201916149

**Materials included in the Thesis are presented at the following scientific events:**

1. D. Cholakova, N. Denkov, S. Tcholakova, I. Lesov, S. Smoukov, "Self-shaping" drops, *Solutions in the Spring* 3-6.04.2016, Homerton College, Cambridge, UK – poster. The poster was rewarded as **"best poster" prize**.
2. Д. Чолакова, Н. Денков, С. Чолакова, И. Лесов, С. Смуков, "Контрол върху формата на капки, претърпяващи фазов преход", *XV National chemistry conference for students and PhD students* 18-20.05.2016, Sofia, Bulgaria – oral presentation.
3. N. Denkov, S. Tcholakova, D. Cholakova, I. Lesov, Zh. Valkova S. K. Smoukov, "Self-shaping droplets: from spheres to platelets with "flagella"", *Flowing Matter*, 23-27.01.2017 г., Porto, Portugal – oral presentation.
4. Д. Чолакова, Ж. Вълкова, С. Чолакова, Н. Денков, С. Смуков, "Енталпийни ефекти при деформирането на емулсионни капки", *XVII National chemistry conference for students and PhD students* 16-18.05.2018, Sofia, Bulgaria – oral presentation.
5. D. Cholakova, N. Denkov, S. Tcholakova, I. Lesov, Z. Valkova, S. Smoukov, „Self-shaping of single and multicomponent droplets via the formation of intermediate rotator phases upon cooling" – *Conference of International Association of Colloid and Interface Scientists* 21-25.05.2018, Rotterdam, Netherlands – oral presentation.
6. D. Cholakova, N. Denkov, S. Tcholakova, Z. Valkova, I. Lesov, S. K. Smoukov, "Self-shaping and self-emulsification of emulsion drops upon cooling and heating" - *STEM Exchange: Research and Career Symposium*, organized by PepsiCo and New York Academy of Sciences 28.08.2018 г., New York, USA – poster.
7. D. Cholakova, N. Denkov, S. Tcholakova, Z. Valkova, I. Lesov, S. Smoukov „Self-shaping of single and multicomponent emulsion drops" – conference *Chemistry today for tomorrow* 01.02.2019 г., Sofia, Bulgaria – oral presentation.
8. D. Cholakova, Z. Valkova, S. Tcholakova, N. Denkov, B. P. Binks, "Self-shaping of emulsion droplets in presence of adsorbed latex particles upon cooling" *17th European Student Colloid Conference* 18-22.06.2019 г., Varna, Bulgaria – oral presentation.
9. N. Denkov, D. Cholakova, S. Tcholakova, S. Smoukov, "Self-shaping droplets: from spheres to platelets with flagella", *8th Conference Bubble & Drop*, 24-28.06.2019 г., Sofia, Bulgaria – keynote presentation.
10. N. Denkov, D. Cholakova, S. Tcholakova, I. Lesov, S. Smoukov, "Self-shaping of oily drops: control,

mechanism, importance", *17th European Student Colloid Conference*, 18-22.06.2019 г., Varna, Bulgaria – plenary talk.

11. Zh. Valkova, D. Cholakova, S. Tcholakova, N. Denkov, S. K. Smoukov, "Multilayer formation in self-shaping emulsion droplets", *Advanced Materials Workshop* 21–25.07.2019 г., St. St Constantin & Helena – oral presentation.

12. D. Cholakova, Z. Valkova, N. Denkov, S. Tcholakova, S. K. Smoukov, "Symmetry break in emulsion droplets of mixed alkanes upon cooling" *33rd European Colloids and Interfaces Society Conference* 9-13.09.2019 г., Leuven, Belgium – oral presentation. The talk has been rewarded with **Enzo Ferroni award for best oral presentation given by a young scientist** on the conference.

13. D. Glushkova, D. Cholakova, S. Tcholakova, Z. Valkova, N. Denkov, S. K. Smoukov, "Multilayer formation in self-shaping drops: DSC & X-ray characterization" *33rd European Colloids and Interfaces Society Conference* 9-13.09.2019 г., Leuven, Belgium – poster presentation.

14. N. Denkov, D. Cholakova, S. Tcholakova, S. Smoukov, "Self-shaping and self-fragmentation of droplets in cooled emulsions: a new approach for fabrication of micro- and nanoparticles of various shapes", *10th National conference in Chemistry*, 26-28.09.2019 г., Sofia, Bulgaria – plenary talk.

**Other papers co-authored by D. Cholakova and connected to the subject of this Thesis:**

1. N. Denkov, S. Tcholakova, I. Lesov, D. Cholakova, S. Smoukov, Self-shaping of oil droplets via the formation of intermediate rotator phases upon cooling, *Nature*, **2015**, *528*, 392-395.
2. P. Haas, R. Goldstein, S. Smoukov, D. Cholakova, N. Denkov, A theory of shape-shifting droplets, *Phys. Rev. Lett.*, **2017**, *118*, 088001-1 – 088001-5.
3. S. Tcholakova, Zh. Valkova, D. Cholakova, Z. Vinarov, I. Lesov, N. Denkov, S. K. Smoukov, Efficient self-emulsification via cooling-heating cycles, *Nat. Commun.*, **2017**, *8*, 15012.
4. Z. Valkova, D. Cholakova, S. Tcholakova, N. Denkov, S. Smoukov, Mechanisms and control of self-emulsification upon freezing and melting of dispersed alkane drops, *Langmuir*, **2017**, *33*, 12155-12170.
5. D. Cholakova, Z. Valkova, S. Tcholakova, N. Denkov, S. Smoukov, Self-shaping of multicomponent drops, *Langmuir*, **2017**, *33*, 5696–5706.
6. D. Cholakova, N. Denkov, Rotator phases in alkane systems: in bulk, surface layers and micro/nano confinements, *Adv. Colloid Interface Sci.*, **2019**, 269, 7-42.
7. P. Haas, D. Cholakova, N. Denkov, R. Goldstein, S. Smoukov, Shape-shifting polyhedral droplets, *Phys. Rev. Research*, **2019**, 1, 023017.
8. N. Denkov, S. Tcholakova, D. Cholakova, Surface phase transitions in foams and emulsions, *Curr. Opin. Colloid Interface Sci.*, **2019**, 44, 32-42.
9. D. Cholakova, Z. Valkova, S. Tcholakova, N. Denkov, B. P. Binks, Spontaneous particle desorption and "Gorgon" drop formation from particle-armored oil drops upon cooling, *Soft Matter,* **2020**.

**Citations – totally 56 citations of the above papers have been noticed so far:**

1. Denkov et al. *Nature,* **2015 –** 40 citations
2. Haas et al. *Phys. Rev. Lett.,* **2017** – 3 citations
3. Tcholakova et al. *Nat. Commun.,* **2017 –** 6 citations
4. Valkova et al. *Langmuir,* **2017** – 1 citation
5. Cholakova et al., *Langmuir,* **2017** – 3 citations
6. Cholakova & Denkov, *Adv. Colloid Interface Sci.,* **2019** – 3 citations